Nuclear Instruments and Methods in Physics Research A 608 (2009) 206–224

Contents lists available at ScienceDirect

Nuclear Instruments and Methods in Physics Research A

journal homepage: www.elsevier.com/locate/nima

Technical Note

The extended-track event reconstruction for MiniBooNE

R.B. Patterson [b,*,1], E.M. Laird [b], Y. Liu [a], P.D. Meyers [b], I. Stancu [a], H.A. Tanaka [b,2]

[a] University of Alabama, Department of Physics and Astronomy, Tuscaloosa, AL 35487, USA
[b] Princeton University, Department of Physics, Joseph Henry Laboratories, Princeton, NJ 08544, USA

ARTICLE INFO

Article history:
Received 5 February 2009
Received in revised form
17 June 2009
Accepted 18 June 2009
Available online 2 July 2009

Keywords:
MiniBooNE
BooNE
Reconstruction
Event reconstruction
Neutral pion
Pi0
Cherenkov detector
Ring Imaging
Neutrino
Neutrino oscillations
Maximum likelihood
Particle identification
PID
Mineral oil

ABSTRACT

The Booster Neutrino Experiment (MiniBooNE) searches for $\nu_\mu \rightarrow \nu_e$ oscillations using the ~1 GeV neutrino beam produced by the FNAL Booster synchrotron. The array of photomultiplier tubes (PMTs) lining the MiniBooNE detector records Cherenkov and scintillation photons from the charged particles produced in neutrino interactions. We describe a maximum likelihood fitting algorithm used to reconstruct the basic properties (position, direction, energy) of these particles from the charges and times measured by the PMTs. The likelihoods returned from fitting an event to different particle hypotheses are used to categorize it as a signal ν_e event or as one of the background ν_μ processes, in particular charged current quasi-elastic scattering and neutral current π^0 production. The reconstruction and event selection techniques described here can be applied to current and future neutrino experiments using similar Cherenkov-based detection.

1. Introduction

Cherenkov detectors of $\gtrsim 1$ kt have played a key role in the establishment of the phenomenon of neutrino oscillations [1a, b, 2a–c, 3a–c]. These detectors typically consist of a large volume of a homogeneous transparent medium (water or mineral oil) with a high index of refraction surrounded by an array of photomultiplier tubes (PMTs). Cherenkov photons produced by charged particles emerging from the neutrino interactions and traversing the medium with $\beta > 1/n$ (where n is the index of refraction and $\beta = v/c$) are detected by the PMTs. The photons are emitted at an angle θ_C relative to the track direction, where $\cos\theta_C = 1/n\beta$. The radiation is azimuthally symmetric about the track direction, resulting in a ring-like pattern that can be identified on the PMT array. The quantity, spatial distribution, and arrival times of these photons provide information on the location, direction, and energy of the particle. We refer to the extraction of such information from the charge and time measurements of the PMTs as "reconstruction." An analysis of the ring profile can also provide information on the identity of the particle and, if multiple rings are detected, the number of particles.

In this paper, we discuss the event reconstruction algorithms used in the Booster Neutrino Experiment (MiniBooNE), which searches for an excess of ν_e interactions indicative of $\nu_\mu \rightarrow \nu_e$ oscillations using the Fermilab ~1 GeV neutrino beam. The MiniBooNE detector is a sphere of radius 610.6 cm filled with Marcol 7 mineral oil ($n \approx 1.47$) and divided into two optically isolated regions by an opaque shell of radius 575 cm, concentric with the sphere. The surface of the inner "main" region is instrumented with an array of 1280 inward-facing 8 in. PMTs which detect the light produced by the neutrino interactions. The outer "veto" region is instrumented with 240 PMTs and is used to tag charged particles that enter the detector from outside (e.g., cosmic muons) or that exit the main region. Though no scintillator was added to the Marcol 7, it scintillates weakly, resulting in the production of delayed isotropic light for particles with sub- and super-Cherenkov velocities. A more detailed description of the experiment can be found in Refs. [4,5].

* Corresponding author.
E-mail address: rbpatter@caltech.edu (R.B. Patterson).
[1] Now at the California Institute of Technology, Physics Department 103-33, Pasadena, CA 91125, USA.
[2] Now at the University of British Columbia, Department of Physics and Astronomy, Vancouver, BC, Canada V6T 1Z1.

0168-9002/$ - see front matter © 2009 Elsevier B.V. All rights reserved.
doi:10.1016/j.nima.2009.06.064

2. Neutrino interactions at MiniBooNE

The ~1 GeV neutrino beam at MiniBooNE results in interactions with relatively low outgoing particle multiplicity. The largest interaction channel is the charged current quasi-elastic (CCQE) process:

$$\nu_\ell + \mathrm{n} \rightarrow \ell^- + \mathrm{p} \tag{1}$$

which accounts for ~40% of all neutrino interactions in the MiniBooNE detector. Since the recoil proton of Eq. (1) is typically below Cherenkov threshold, only the outgoing lepton produces significant light. In modeling such events within a reconstruction algorithm, one can therefore consider only the Cherenkov and scintillation light produced by the outgoing lepton. While the recoiling nucleon can produce scintillation light, this additional source of light is not considered in the reconstruction.

A muon in the MiniBooNE detector exhibits minimum-ionizing behavior through most of its path with little chance of radiative energy loss. In contrast, electrons typically induce electromagnetic showers, resulting in additional electrons and positrons that emit Cherenkov light. Thus, muons and electrons have significantly different Cherenkov ring patterns. This difference is the basis for distinguishing a muon track from an electron track, and the reconstruction algorithm has a model for each.

The next most abundant process in MiniBooNE is single pion production, which occurs primarily via Δ resonance or coherent scattering:

$$\nu_\ell + N \rightarrow \ell^- + N' + \pi \quad (\mathrm{CC}\ \pi)$$

$$\nu_\ell + N \rightarrow \nu_\ell + N' + \pi \quad (\mathrm{NC}\ \pi) \tag{2}$$

where $N^{(\prime)}$ denotes a nucleon in the case of resonance production and a nucleus in the case of coherent production. Of particular interest is neutral current (NC) π^0 production. The two photons from $\pi^0 \rightarrow \gamma\gamma$ decay induce electromagnetic showers indistinguishable in MiniBooNE from those induced by electrons. Since the recoil nucleon/nucleus is typically below Cherenkov threshold, these NC π^0 events are well described in the reconstruction algorithm by two electron-like tracks pointing back to a common vertex. The presence of two distinct Cherenkov rings allows for the separation of π^0 events from electron (ν_e CCQE) events. However, π^0 misidentification (for example, due to a large energy asymmetry between the two photons or due to a small photon opening angle which leaves the Cherenkov rings overlapping) accounts for most of the reducible background in the $\nu_\mu \rightarrow \nu_e$ oscillation search. Thus, successful reconstruction and identification of π^0 events is critical.

While other channels can be accommodated by the reconstruction algorithm, the ν_e appearance oscillation analysis uses only four event models: single electron track, single muon track, two γ tracks, and two γ tracks with a π^0 invariant mass.

3. The detector response

The Marcol 7 mineral oil used in MiniBooNE exhibits a rich array of optical phenomena despite its ~20 m extinction length near the peak of PMT sensitivity (~400 nm). Cherenkov and scintillation light production is accompanied by photon absorption, fluorescence (with several possible excitation/emission spectra and lifetimes), and Rayleigh and Raman scattering. The left plot in Fig. 1 summarizes the rates of various processes as a function of wavelength. The cumulative extinction rate is shown as the black line. In the near-ultraviolet region (<320 nm), fluorescence processes dominate the extinction rate. The fluorescence lifetimes range from 1 to 35 ns. In the visible region (>320 nm), the dominant processes are Rayleigh scattering and absorption.

The 1520 8 in. PMTs in MiniBooNE are of two types: 322 model R5912 PMTs and 1198 model R1408 PMTs, both from Hamamatsu. All of the R5912 PMTs are located in the main PMT array. The PMT time response (particularly the late-pulsing behavior) and the variation of PMT efficiency with incident angle have been characterized in external measurements using a pulsed LED [6]. The PMTs *in situ* have been studied using a laser calibration system that produces sub-nanosecond bursts of nearly isotropic light in the detector.

The right panel of Fig. 1 shows the times of PMT hits recorded in laser calibration events relative to their expected times. The colored histograms come from Monte Carlo simulation, with the red curve showing PMT and electronics timing effects (including pre- and late-pulsing), the green curve including photon scattering, and the blue curve adding photon reflections from the PMTs and the surface of the main detector region. The resulting time structure matches well with that seen in data (black points). We note that only the earliest photoelectron's time is reported when

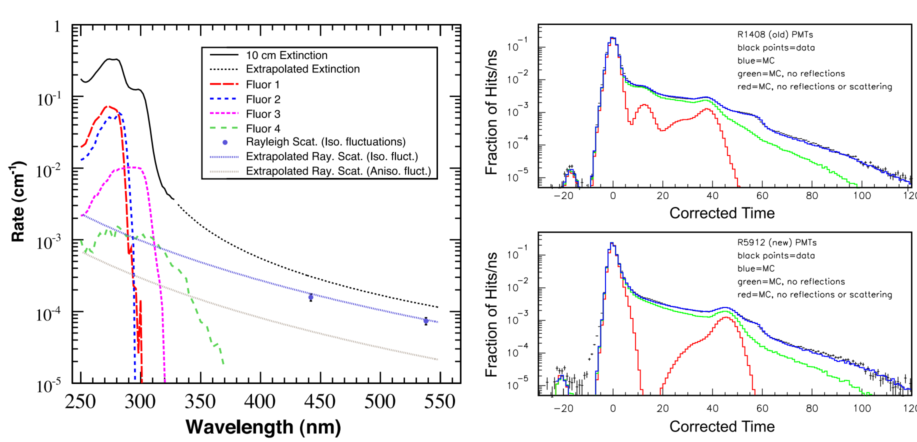

Fig. 1. Left: rates of optical processes in Marcol 7 as a function of wavelength. The solid black line is the overall extinction rate obtained from laboratory measurements. The dashed black line is the extrapolated rate based on *in situ* data. The curves labeled "Fluor *n*" are the excitation rates for the four identified fluorescence processes. The light blue points represent the measured rates of Rayleigh scattering, and the dashed light blue and gray lines represent extrapolated rates. Right: reconstructed photon arrival times for R1408 (top) and R5912 (bottom) PMTs for 397 nm light flashed from the center of the detector. The black histogram is the distribution from data and the blue is the complete Monte Carlo simulation. The green (red) shows the simulation with reflections (and scattering) turned off. (For interpretation of the references to color in this figure legend, the reader is referred to the web version of this article.)